Journal of the Mechanics and Physics of Solids 60 (2012) 1771–1790

Contents lists available at SciVerse ScienceDirect

Journal of the Mechanics and Physics of Solids

journal homepage: www.elsevier.com/locate/jmps

Micro-buckling in the nanocomposite structure of biological materials

Yewang Su [a], Baohua Ji [a,b,*], Keh-Chih Hwang [a], Yonggang Huang [c,**]

[a] AML, Department of Engineering Mechanics, Tsinghua University, Beijing 100084, PR China
[b] Biomechanics and Biomaterials Laboratory, Department of Applied Mechanics, School of Aerospace Engineering, Beijing Institute of Technology, Beijing 100081, PR China
[c] Department of Civil and Environmental Engineering and Mechanical Engineering, Northwestern University, Evanston, IL 60208, USA

ARTICLE INFO

Article history:
Received 25 October 2011
Received in revised form
19 March 2012
Accepted 22 May 2012
Available online 4 June 2012

Keywords:
Biological materials
Buckling strength
Flaw insensitivity
Staggered alignment
Aspect ratio

ABSTRACT

Nanocomposite structure, consisting of hard mineral and soft protein, is the elementary building block of biological materials, where the mineral crystals are arranged in a staggered manner in protein matrix. This special alignment of mineral is supposed to be crucial to the structural stability of the biological materials under compressive load, but the underlying mechanism is not yet clear. In this study, we performed analytical analysis on the buckling strength of the nanocomposite structure by explicitly considering the staggered alignment of the mineral crystals, as well as the coordination among the minerals during the buckling deformation. Two local buckling modes of the nanostructure were identified, i.e., the symmetric mode and anti-symmetric mode. We showed that the symmetric mode often happens at large aspect ratio and large volume fraction of mineral, while the anti-symmetric happens at small aspect ratio and small volume fraction. In addition, we showed that because of the coordination of minerals with the help of their staggered alignment, the buckling strength of these two modes approached to that of the ideally continuous fiber reinforced composites at large aspect ratio given by Rosen's model, insensitive to the existing "gap"-like flaws between mineral tips. Furthermore, we identified a mechanism of buckling mode transition from local to global buckling with increase of aspect ratio, which was attributed to the biphasic dependence of the buckling strength on the aspect ratio. That is, for small aspect ratio, the local buckling strength is smaller than that of global buckling so that it dominates the buckling behavior of the nanocomposite; for comparatively larger aspect ratio, the local buckling strength is higher than that of global buckling so that the global buckling dominates the buckling behavior. We also found that the hierarchical structure can effectively enhance the buckling strength, particularly, this structural design enables biological nanocomposites to avoid local buckling so as to achieve global buckling at macroscopic scales through hierarchical design. These features are remarkably important for the mechanical functions of biological materials, such as bone, teeth and nacre, which often sustain large compressive load.

* Corresponding author at: Biomechanics and Biomaterials Laboratory, Department of Applied Mechanics, School of Aerospace Engineering, Beijing Institute of Technology, Beijing 100081, PR China.
** Corresponding author at: Department of Civil and Environmental Engineering and Mechanical Engineering, Northwestern University, Evanston, IL 60208, USA.
E-mail addresses: bhji@bit.edu.cn, bhji@mail.tsinghua.edu.cn (B. Ji), y-huang@northwestern.edu (Y. Huang).

0022-5096/$ - see front matter © 2012 Elsevier Ltd. All rights reserved.
http://dx.doi.org/10.1016/j.jmps.2012.05.003

1. Introduction

Biological composite materials have attracted intensive attention of scientific research due to their superior mechanical properties (Currey, 1977; Fratzl and Weinkamer, 2007; Gao et al., 2003; Jackson et al., 1988; Jager and Fratzl, 2000; Ji and Gao, 2004b; Su, 2010). They are thought as excellent model systems for synthesis of advanced nanocomposites. For example, tooth and bone have a combination of high hardness and high strength for cutting the food and for supporting the weight of animals, respectively. Nacre has high strength in both compression and bending for protecting animals from the attack of predators (Katti et al., 2001). Mechanical principles inspired by these biological materials were recently proposed regarding the effect of length scale, geometry of microstructure and levels of hierarchy on optimization of the hardness, strength and toughness of these materials (Gao, 2006; Ji and Gao, 2010; Zhang et al., 2011). Although these biological materials have various macroscopic structures with different levels of hierarchy and mechanical functions, they often process a convergent nanocomposite structure as their basic building block (Gupta et al., 2006; Jager and Fratzl, 2000; Kamat et al., 2000; Landis, 1995; Landis et al., 1996; Rho et al., 1998; Tesch et al., 2001; Wang et al., 2001; Warshawsky, 1989) (see Fig. 1). This exquisite nanostructure consists of mineral crystals with a large aspect ratio embedded in the protein matrix in a staggered manner. Its mechanical features has been depicted by the so-called tension-shear chain (TSC) model proposed by Gao et al. (2003), i.e., the mineral crystals bear most of the tensile or compressive load, while the protein matrix transfers forces between adjacent crystals via shear. The TSC model has been serving as a basic model for understanding the mechanical properties, such as the fracture strength, toughness, hardness, and elastic stability, etc., of biological and biomimicking nanocomposites (Bonderer et al., 2008; Dashkovskiy et al., 2007; Fang et al., 2007; Gao, 2006; He and Swain, 2007; Ji and Gao, 2004a, 2006; Katti and Katti, 2006; Kauffmann et al., 2005; Mayer, 2005; Zuo and Wei, 2008).

In contrast to the studies of hardness, strength and toughness, those on the buckling behaviors of the biological nanocomposites are comparatively less. However, because the mineral crystals have slender geometry with large aspect ratio, they are susceptible to buckling under the compressive load. Meyer and coworkers (Menig et al., 2000, 2001) carried out compression tests on sea shells samples (from conch and abalone) and found that local buckling and kinking occurs in the lamellar structures of the samples. Ji et al. (2004) performed a preliminary analysis on the compressive strength of the nanocomposite structure of biological materials. In their study, they analyzed the local buckling behavior of a single

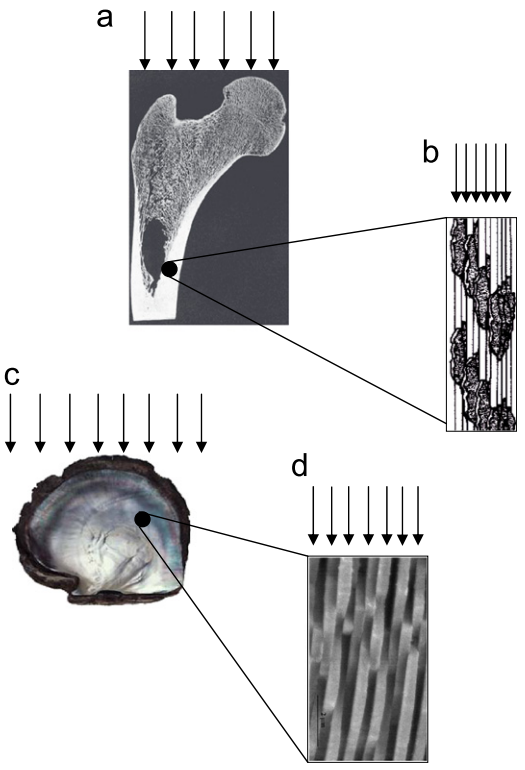

Fig. 1. Biological materials and their nanocomposite structures. (a) Macroscopic bone tissue under compressive loading; (b) the nanostructure of bone made up of plate-like crystals (2–4 nm thick, up to 100 nm long) embedded in a protein matrix; (c) macroscopic nacre under pressure; (d) the nanostructure of nacre made up of plate-like crystals (200–500 nm thick and a few micrometers long) with very thin protein matrix. These nanocomposite structures share a "brick-and-motar" like structural feature of hard platelets with very large aspect ratio arranged in a staggered manner in soft matrix.

mineral crystal in the nanostructure by assuming that its neighboring crystals were rigid so that they acted as strong confinement on this single crystal. They showed that there exists a transition of buckling strength from an aspect-ratio-dependent regime of compressive strength to a lower threshold value independent of the crystal geometry. They found that the typical values of aspect ratio of mineral crystals of bone and nacre fall in this transition region. Although this study provided some insights into the compressive strength of the nanostructure of biological materials, one weakness of this analysis (Ji et al., 2004) is that they did not consider possible coordination among the adjacent minerals during buckling deformation, therefore the buckling strength they obtained corresponds to the higher order buckling modes.

Rosen (1964) analyzed the elastic buckling of ideally continuous fibers reinforced composites considering coordination between the continuous fibers. He showed that the composites normally exhibit two kinds of buckling modes: the tension buckling mode (TBM) where the fibers in matrix exhibit anti-phase deformation, and the shear buckling mode (SBM) where the fibers exhibit in-phase deformation. The tension mode occurs for relatively low fiber volume fraction, while the shear mode takes place for larger volume fraction. Since then, many studies followed (Guz and Checkhov, 1992; Hull, 1981; Jones, 1975; Schuerch, 1966). Recently, Parnes and Chiskis (2002) re-studied the two buckling modes by employing more rigorous analysis. They showed that the buckling stress of the TBM is always larger than that of the SBM. In addition, in the case of dilute composites, the TBM stress was seen to converge to the SBM one. In particular, they showed that while the SBM exhibited infinite wavelengths in the non-dilute composites, it had finite wavelengths in the dilute composites. In above studies, the fibers were all considered as continuous and infinite long. Therefore, the method as well as the results of these studies cannot be applied to the analysis of buckling behaviors of the nanocomposite structure of biological materials which features a unique staggered alignment of mineral of finite length in the protein matrix.

Regarding the unique microstructure of biological materials, several basic scientific questions have remained unresolved, e.g., how to model the effect of coordination among the staggered minerals, and what are the roles of the coordination of minerals as well as the structural hierarchy in the buckling strength of biological materials? In this paper, a theoretical model considering the staggered alignment of mineral was developed for studying the buckling behaviors of the nanocomposite structure of biological materials. One special interest is to focus on the effect of the coordination among neighboring mineral crystals on the buckling behaviors because of this unique arrangement of minerals. This study would be helpful for understanding of the mechanical strength of biological materials by considering micro-buckling as a possible failure mechanism. The minerals were modeled as Euler beams while the protein matrix as elastic substrate providing both shear and lateral confinement to the minerals and coordinating their buckling deformation. The challenge is that the complex arrangement of minerals poses an enormous difficulty to the analytical analysis. Here the perturbation method and energy method were adopted for deriving the critical buckling modes and strength. Two local buckling modes of the nanostructure were studied, i.e., the symmetric mode and the anti-symmetric mode. The effect of the geometry and volume fraction of mineral crystals on the competition between the symmetric and anti-symmetric modes was analyzed. Furthermore, the role of the structural hierarchy in buckling behaviors of biological nanocomposites was discussed.

2. The model

Fig. 2a depicts the "brick-and-motar" like nanostructure of biological nanocomposites where the mineral crystals align in the protein matrix in a staggered manner. To study the buckling behaviors of the nanostructure, one representative unit

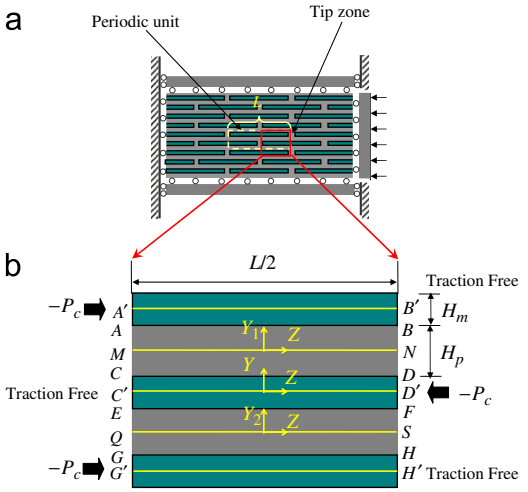

Fig. 2. Theoretical model of the nanocomposite structure of biological materials. (a) The brick-and-motar-like nanocomposite structure in which the mineral crystals align in the protein matrix in a staggered manner. A periodic structural unit is identified by a dashed rectangle; (b) the simplified model consisting of one half of the periodic unit plus one half mineral of its neighboring periodic unit, where the tip zones are modeled by crack-like traction free surfaces.

cell can be extracted as shown in the dotted line. We consider one half of the periodic unit (because it is symmetric about its Y axis) plus one more half of mineral in the neighboring unit (see Fig. 2a and b). For simplicity, a uniform compressive displacement load on the nanocomposite was assumed. This assumption can be justified as follows:

(1) Firstly, the nanostructures we are considering are far enough from the loading position of the macroscopic force, where the effect of non-uniformity of the macroscopic force will be largely attenuated at the position we are interested according to Saint-Venant's Principle.
(2) Secondly, the nanostructure and its higher level structure where it was embedded are 7–8 orders of magnitude smaller than the macroscopic scales of biological materials, therefore the spatial non-uniform distribution of loading at macroscale will be largely smoothed down at the nanoscale.
(3) Thirdly, regarding the effect of structural gradation on the loading distribution, it has been shown that the unique deformation mechanisms of biological materials can induce an approximately uniform deformation transformation from the high level to the low level scales with the help of its hierarchical gradation. For example, Gupta et al. (2005, 2006) showed that the deformation of a bone sample at tissue level (millimeter scale) under a uniaxial loading can have an uniformly distributed deformation of the embedded mineralized fibrils (100 nm level) at different position of the tissue sample (across a length scale of 5 mm), as well as the uniformly distributed deformation of minerals (a few nanometers) at different position of mineralized fibrils. Therefore, our assumption about the uniform displacement loading condition on the nanostructure and its unit cell is reasonable and supported by the experimental observations.

Furthermore, according to the TSC model, the role of protein in the tip zone between the mineral tips (see Fig. 2a) can be neglected due to the softness of protein compared with the mineral (modulus ratio between them is as high as 3 orders of magnitude) and due to the relative small size of the tip zone compared with the length of the mineral (Gao et al., 2003). Therefore, the tip zones are equivalent to crack-like traction free surfaces, and our model is then simplified to Fig. 2b. In this study, the mineral crystals are modeled as Euler–Bernoulli beams, denoted by $A'B'$, $C'D'$, and $G'H'$, where $G'H'$ is the repeat of $A'B'$ in the neighboring periodic unit. The protein matrix acts as a 2D elastic support through both shear and normal deformation. The two blocks of protein matrix are denoted by *ABCD* and *EFGH*. For simplicity of analysis, here we assume that the relative displacement of the tips of two neighboring minerals is smaller than the size of the tip zone so that the traction free condition is always satisfied during the buckling analysis of the nanostructure. This assumption will be further justified later in the discussion.

3. Static analysis of the nanocomposite structure

To begin with, we derive the static stress field in the nanostructure under a uniaxial load before the buckling. According to the TSC model, the protein matrix transfers load between adjacent mineral crystals through shear deformation, as depicted in Fig. 3. Assuming that the shear deformation in protein matrix is uniform along the Y_1 direction (thickness), the shear strain in protein *ABCD* is obtained as,

$$\mathring{\gamma}_{YZ}(Z)=\frac{\mathring{u}_3^{A'B'}(Z)-\mathring{u}_3^{C'D'}(Z)}{H_p} \tag{1}$$

where H_p is the thickness of protein. The superscript $\circ$ denotes the values before buckling, and the subscript "3" denotes the Z direction. Similarly, subscript "1" and "2" denote X and Y directions, respectively, in the following derivations. Because of the symmetry, the shear strain in protein *EFGH* is equal to $\mathring{\gamma}_{YZ}(Z)$. The shear stress and strain obey Hooke's law as,

$$\mathring{\tau}_{YZ}(Z)=G_p\mathring{\gamma}_{YZ}(Z) \tag{2}$$

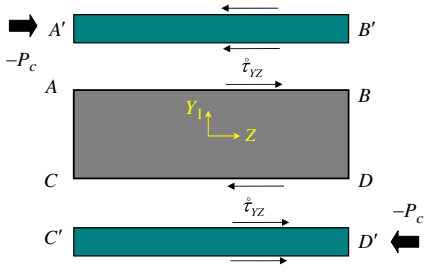

Fig. 3. Schematic illustration of the shear stress at the interface between minerals ($A'B'$ and $C'D'$) and protein matrix (*ABCD*) along the longitudinal direction of mineral.

and the axial force in mineral is

$$\begin{cases} \overset{\circ}{t}_3^{A'B'}(Z) = E_m H_m \frac{d\overset{\circ}{u}_3^{A'B'}(Z)}{dZ} \\ \overset{\circ}{t}_3^{C'D'}(Z) = E_m H_m \frac{d\overset{\circ}{u}_3^{C'D'}(Z)}{dZ} \end{cases} \tag{3}$$

where G_p and E_m are the shear modulus of protein and Young's modulus of mineral, respectively. H_m denotes the thickness of mineral crystal.

According to the equilibrium of mineral, we have

$$\begin{cases} \frac{1}{2}\frac{d\overset{\circ}{t}_3^{A'B'}(Z)}{dZ} - \overset{\circ}{\tau}_{YZ}(Z) = 0 \\ \frac{1}{2}\frac{d\overset{\circ}{t}_3^{C'D'}(Z)}{dZ} + \overset{\circ}{\tau}_{YZ}(Z) = 0 \end{cases} \tag{4}$$

where the boundary conditions at the ends of the beams $A'B'$ and $C'D'$ are

$$\begin{cases} \overset{\circ}{t}_3^{A'B'}(-\frac{L}{4}) = P_c, \quad \overset{\circ}{t}_3^{A'B'}(\frac{L}{4}) = 0 \\ \overset{\circ}{t}_3^{C'D'}(-\frac{L}{4}) = 0, \quad \overset{\circ}{t}_3^{C'D'}(\frac{L}{4}) = P_c \end{cases} \tag{5}$$

in which P_c is the given axial load. The positive value means tension, while the negative means compression. The distribution of the axial force in mineral can be solved as,

$$\overset{\circ}{t}_3^{A'B'}(Z) = \frac{P_c}{2}\left(1 - \frac{sh(kZ)}{sh(kL/4)}\right) \tag{6a}$$

$$\overset{\circ}{t}_3^{C'D'}(Z) = \frac{P_c}{2}\left(1 + \frac{sh(kZ)}{sh(kL/4)}\right) \tag{6b}$$

where $k = \sqrt{4G_p/(E_m H_m H_p)}$.

The shear stress in protein *ABCD* and *EFGH* is obtained as

$$\overset{\circ}{\tau}_{YZ}(Z) = -\frac{P_c k}{4}\frac{ch(kZ)}{sh(kL/4)} \tag{7}$$

For the convenience of derivation, we rewrite Eqs. (6a), (6b) and (7) as

$$\overset{\circ}{\tilde{t}}_3^{A'B'}(\xi) = \frac{P_c}{2}\left(1 - \frac{sh(\gamma\xi)}{sh(\gamma/4)}\right) \tag{8a}$$

$$\overset{\circ}{\tilde{t}}_3^{C'D'}(\xi) = \frac{P_c}{2}\left(1 + \frac{sh(\gamma\xi)}{sh(\gamma/4)}\right) \tag{8b}$$

$$\overset{\circ}{\tilde{\tau}}_{YZ}(\xi) = -\frac{P_c\gamma}{4L}\frac{ch(\gamma\xi)}{sh(\gamma/4)} \tag{9}$$

where $\gamma = \sqrt{2\rho^2 V_m/[\kappa(1+\nu_p)(1-V_m)]}$ is a dimensionless parameter composed of geometrical and material parameters of the nanocomposite structure, where $\kappa = E_m/E_p$, $\rho = L/H_m$ and $V_m = H_m/(H_m+H_p)$ are modulus ratio, aspect ratio and volume fraction of mineral, respectively. In addition, $\xi = Z/L$ denotes the normalized coordinate of Z. Note that the axial force $\overset{\circ}{\tilde{t}}_3^{A'B'}(\xi) = \overset{\circ}{t}_3^{A'B'}(Z)$, $\overset{\circ}{\tilde{t}}_3^{C'D'}(\xi) = \overset{\circ}{t}_3^{C'D'}(Z)$ and shear stress $\overset{\circ}{\tilde{\tau}}_{YZ}(\xi) = \overset{\circ}{\tau}_{YZ}(Z)$ are obtained by simply substituting $Z = \xi L$ into $\overset{\circ}{t}_3^{A'B'}(Z)$, $\overset{\circ}{t}_3^{C'D'}(Z)$ and $\overset{\circ}{\tau}_{YZ}(Z)$. This notation is also applicable to other functions in the following derivation.

Eqs. (8) and (9) show that the distribution of axial force and shear stress along the longitudinal direction of mineral is in hyperbolic functions, determined by the parameter γ. According to the recent study (Liu et al., 2011), when $\gamma < 4$, as in the cases of biological materials, such as nacre and bone ($\rho \approx 10$–40, $E_m/E_p \approx 1000$), the shearing stress is approximately a constant along the longitudinal direction, and the axial force is approximately linearly distributed along the length of mineral (as shown in Fig. 4), consistent with the assumption made in previous works (Gao et al., 2003).

4. Buckling analysis

4.1. Deformation energy of the system

4.1.1. Total energy of the system before buckling

The total energy of the system before buckling is composed of

$$\overset{\circ}{U} = \overset{\circ}{U}_m + \overset{\circ}{U}_s \tag{10}$$

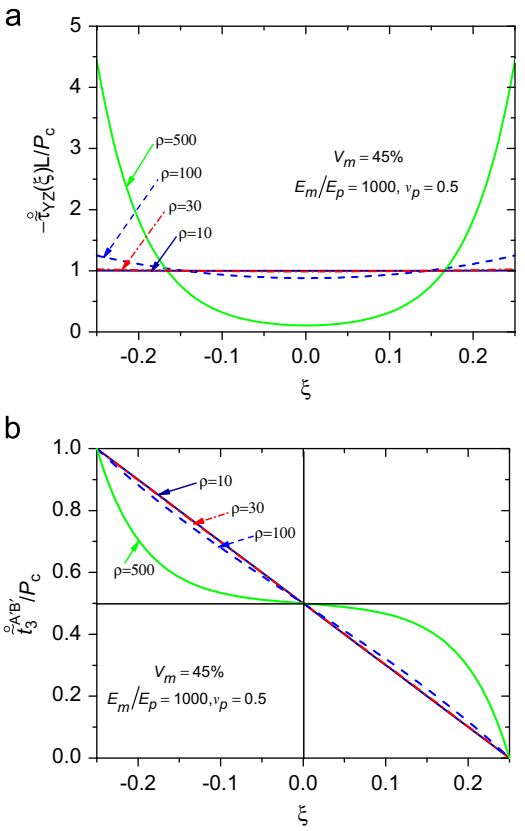

Fig. 4. Illustration of the distribution of (a) the shear stress and (b) the axial force of mineral along its longitudinal direction for different aspect ratio of mineral.

where $\mathring{U}_m$ is the membrane energy of mineral $A'B'$ and $C'D'$ (see Fig. 2),

$$\mathring{U}_m = 2\int_{-L/4}^{L/4} \frac{1}{2E_m H_m} (\mathring{t}_3^{A'B'}(Z))^2\, dZ = \frac{P_c^2 \rho}{4E_m}\left(\frac{1}{2} + \frac{1}{\gamma sh^2(\gamma/4)}\left(sh\left(\frac{\gamma}{4}\right)ch\left(\frac{\gamma}{4}\right) - \frac{\gamma}{4}\right)\right) \tag{11a}$$

and $\mathring{U}_s$ is the shear deformation energy of protein of *ABCD* and *EFGH* (see Fig. 2),

$$\mathring{U}_s = 2\int_{-L/4}^{L/4} \frac{H_p}{2G_p}\left(\mathring{\tau}_{YZ}^{AB}(Z)\right)^2 dZ = \frac{P_c^2\gamma(1-V_m)}{16sh^2(\gamma/4)\rho V_m G_p}\left(sh\left(\frac{\gamma}{4}\right)ch\left(\frac{\gamma}{4}\right) + \frac{\gamma}{4}\right) \tag{11b}$$

4.1.2. *Total energy of the system after buckling*

The total energy of the buckled system is

$$U = U_m + U_b + U_s + U_T \tag{12}$$

where U_m and U_b are the membrane energy and bending energy of mineral, respectively, while U_s and U_T are the shear deformation energy and tension deformation energy of protein, respectively. These energy terms will be derived as follows.

We assume the incremental buckling deformation of minerals $A'B'$, $C'D'$ and $G'H'$ in Y direction (see Fig. 2) as

$$\begin{cases} u_2^{A'B'}(Z) = v_1(Z) + C_1 \\ u_2^{C'D'}(Z) = v_2(Z) \\ u_2^{G'H'}(Z) = v_1(Z) + C_2 \end{cases} \tag{13}$$

where C_1 and C_2 are constant, representing the displacements of minerals $A'B'$ and $G'H'$ at A' and G' in Y direction, respectively, on the condition of $v_1(Z = -L/4) = 0$. Because we adopt the displacement loading method in this work, the incremental displacement of minerals in Z direction is negligible.

The displacement in protein matrix can be derived based on the deformation of the mineral. According to the continuity of the displacement field at the mineral–protein interface, the deformation of protein in Y direction at the interface can be

derived as

$$\begin{cases} u_2^{AB}(Z) = v_1(Z) + C_1 \\ u_2^{CD}(Z) = v_2(Z) \\ u_2^{EF}(Z) = v_2(Z) \\ u_2^{GH}(Z) = v_1(Z) + C_2 \end{cases} \tag{14a}$$

while the incremental displacements of the interface in Z direction are mainly produced by the bending deformation of the beams (Parnes and Chiskis, 2002) as,

$$\begin{cases} u_3^{AB}(Z) = \frac{H_m}{2}\frac{d}{dZ}u_2^{A'B'}(Z) = \frac{H_m}{2}v_1'(Z) \\ u_3^{CD}(Z) = -\frac{H_m}{2}\frac{d}{dZ}u_2^{C'D'}(Z) = -\frac{H_m}{2}v_2'(Z) \\ u_3^{EF}(Z) = \frac{H_m}{2}\frac{d}{dZ}u_2^{C'D'}(Z) = \frac{H_m}{2}v_2'(Z) \\ u_3^{GH}(Z) = -\frac{H_m}{2}\frac{d}{dZ}u_2^{G'H'}(Z) = -\frac{H_m}{2}v_1'(Z) \end{cases} \tag{14b}$$

Now we derive the strain and stress fields in the buckled mineral and protein. Because the length of projection of the mineral in Z direction is constant considering the displacement loading condition, the total membrane strain in mineral due to the bending (which elongates the arc length of mineral) is

$$\begin{cases} \varepsilon_m^{A'B'}(Z) = \varepsilon_m^{\circ A'B'}(Z) + \frac{1}{2}\left(\frac{d}{dZ}u_2^{A'B'}(Z)\right)^2 \\ \varepsilon_m^{C'D'}(Z) = \varepsilon_m^{\circ C'D'}(Z) + \frac{1}{2}\left(\frac{d}{dZ}u_2^{C'D'}(Z)\right)^2 \end{cases} \tag{15a}$$

and the curvature (Su, 2012) is

$$\begin{cases} \kappa_m^{A'B'}(Z) = \frac{d^2}{dZ^2}u_2^{A'B'}(Z) \\ \kappa_m^{C'D'}(Z) = \frac{d^2}{dZ^2}u_2^{C'D'}(Z) \end{cases} \tag{15b}$$

The stress in protein $ABCD$ in Y direction is assumed as constant because of its small thickness compared with its length, and could be estimated as the average of the stress of the protein–mineral interfaces AB and CD as

$$\begin{cases} \tau_{ZY}^{AD}(Z) = G_p[\frac{1}{2}(\frac{d}{dZ}u_2^{AB}(Z) + \frac{d}{dZ}u_2^{CD}(Z)) + \frac{1}{H_p}(u_3^{AB}(Z) - u_3^{CD}(Z))] \\ \sigma_{YY}^{AD}(Z) = \frac{E_p}{1-{v_p}^2}\frac{u_2^{AB}(Z) - u_2^{CD}(Z)}{H_p} \end{cases} \tag{16a}$$

Similarly, the stress field in protein $EFGH$ was derived as

$$\begin{cases} \tau_{ZY}^{EH}(Z) = G_p[\frac{1}{2}(\frac{d}{dZ}u_2^{EF}(Z) + \frac{d}{dZ}u_2^{GH}(Z)) + \frac{1}{H_p}(u_3^{EF}(Z) - u_3^{GH}(Z))] \\ \sigma_{YY}^{EH}(Z) = \frac{E_p}{1-{v_p}^2}\frac{u_2^{EF}(Z) - u_2^{GH}(Z)}{H_p} \end{cases} \tag{16b}$$

Once we obtain the stress field in mineral and protein, the elastic energy of the system can be derived as follows. The membrane energy of mineral is given by

$$U_m = \int_{-L/4}^{L/4} \frac{E_m H_m}{2}(\varepsilon_m^{A'B'}(Z)^2 + \varepsilon_m^{C'D'}(Z)^2)dZ \tag{17a}$$

and the bending energy of mineral is

$$U_b = \int_{-L/4}^{L/4} \frac{E_m H_m^3}{24}(\kappa_m^{A'B'}(Z)^2 + \kappa_m^{C'D'}(Z)^2)dZ \tag{17b}$$

Also, the shear energy of protein is given by

$$U_s = \int_{-H_p/2}^{H_p/2}\int_{-L/4}^{L/4} \frac{1}{2G_p}\left(\tau_{YZ}^{\circ AD}(Z) + \tau_{ZY}^{AD}(Z)\right)^2 dZ\,dY + \int_{-H_p/2}^{H_p/2}\int_{-L/4}^{L/4} \frac{1}{2G_p}\left(\tau_{YZ}^{\circ EH}(Z) + \tau_{ZY}^{EH}(Z)\right)^2 dZ\,dY \tag{17c}$$

and the tension energy of protein is

$$U_T = \int_{-H_p/2}^{H_p/2}\int_{-L/4}^{L/4} \frac{1-v_p^2}{2E_p}(\sigma_{YY}^{AD}(Z))^2 dZ\,dY + \int_{-H_p/2}^{H_p/2}\int_{-L/4}^{L/4} \frac{1-v_p^2}{2E_p}(\sigma_{YY}^{EH}(Z))^2 dZ\,dY \tag{17d}$$

Because the work done by external load is zero considering the displacement loading condition, we have $U = \overset{\circ}{U}$, i.e.

$$(U_m - \overset{\circ}{U}_m) + U_b + (U_s - \overset{\circ}{U}_s) + U_T = 0 \tag{18}$$

Substituting Eqs. (15) and (16) into the corresponding equations of Eqs. (17) and (18), we obtain the equation for the critical load P_c of buckling as,

$$\frac{P_c}{4L}h_m+\frac{E_mH_m^3}{24L^3}h_b+\frac{G_p(H_m+H_p)^2}{4H_pL}h_s+\frac{E_pL}{2H_p(1-v_p^2)}h_T=0 \tag{19}$$

where

$$\begin{aligned}
h_m &= \int_{-1/4}^{1/4}\left(\left(\left(\frac{d}{d\xi}\tilde{v}_1(\xi)\right)^2+\left(\frac{d}{d\xi}\tilde{v}_2(\xi)\right)^2\right)-\frac{sh(\gamma\xi)}{sh(\gamma/4)}\left(\left(\frac{d}{d\xi}\tilde{v}_1(\xi)\right)^2-\left(\frac{d}{d\xi}\tilde{v}_2(\xi)\right)^2\right)\right)d\xi\\
h_b &= \int_{-1/4}^{1/4}\left(\frac{d^2}{d\xi^2}\tilde{v}_1(\xi)\right)^2+\left(\frac{d^2}{d\xi^2}\tilde{v}_2(\xi)\right)^2 d\xi\\
h_s &= \int_{-1/4}^{1/4}\left(\frac{d}{d\xi}\tilde{v}_1(\xi)+\frac{d}{d\xi}\tilde{v}_2(\xi)\right)^2 d\xi\\
h_T &= \int_{-1/4}^{1/4}(\tilde{v}_1(\xi)-\tilde{v}_2(\xi)+C_1)^2+(\tilde{v}_1(\xi)-\tilde{v}_2(\xi)+C_2)^2\,d\xi
\end{aligned} \tag{20}$$

in which $\tilde{v}_1(\xi)=v_1(Z)$ and $\tilde{v}_2(\xi)=v_2(Z)$. If we define

$$\overline{\sigma}_c=-\frac{P_c}{2E_p(H_m+H_p)} \tag{21}$$

as the normalized critical stress, then we have the expression of $\overline{\sigma}_c$ from Eq. (19) as,

$$\overline{\sigma}_c=\frac{\frac{E_mH_m^3}{12E_pL^2(H_m+H_p)}h_b+\frac{G_p(H_m+H_p)}{2E_pH_p}h_s+\frac{L^2}{H_p(H_m+H_p)(1-v_p^2)}h_T}{h_m} \tag{22}$$

4.2. Buckling strength

Before we calculate the buckling strength of the nanocomposite structure, the buckling deformation of the mineral and protein has to be determined. Because of the complex staggered alignment of mineral, the estimation of the trial functions of v_1 and v_2 in Eqs. (13) and (14) is not a trivial task. Here we first adopted the energy variation method to obtain the equilibrium governing equation (see Section S.1 in Supporting information), and then we solved its initial perturbation solution using the perturbation method, by which we obtained two buckling modes, one is the symmetric mode and the other is the anti-symmetric mode (see Section S.2 in Supporting information). In order to verify our perturbation solution, we further adopted the numerical simulation method to directly solving the governing equations (see Section S.3 and Fig. S1 in Supporting information) and got the two buckling modes as well, which supports the perturbation solution.

4.2.1. Symmetric buckling mode

Based on the initial solution of the symmetric buckling mode Eqs. (S14) and (S5) (Section S.1 in Supporting information) and numerical simulation results (Section S.3 and Fig. S2 in Supporting information), we assume the buckling mode of

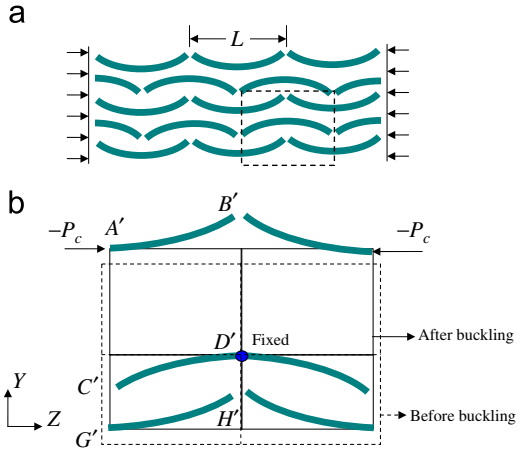

Fig. 5. Illustration of the symmetric mode of local buckling of mineral in the nanocomposite structure. (a) Buckling deformation pattern in a periodic manner and (b) illustration of equilibrium analysis of minerals under the axial loading in one periodic structure unit.

minerals $A'B'$ and $C'D'$ (see Fig. 5) as

$$\begin{cases} \tilde{v}_1(\xi) = -A\sin 2\pi\xi + B\cos\pi(\xi+\frac{1}{4}) - (A+B) \\ \tilde{v}_2(\xi) = -A\sin 2\pi\xi - B\cos\pi(\xi-\frac{1}{4}) + (A+B) \end{cases} \tag{23}$$

where the parameters C_1, C_2, A and B will be determined using the energy method.

Substituting Eq. (23) into Eq. (20), we have

$$h_m = \pi\left(2\pi A^2 + \frac{16}{3}AB + \frac{1}{2}\pi B^2\right) - 2\pi^2\left(8\pi\frac{(\gamma^2+3\pi^2)-2\pi\gamma\coth(\gamma/4)}{(\gamma^2+\pi^2)(\gamma^2+9\pi^2)}AB + \frac{\gamma\coth(\gamma/4)}{\gamma^2+4\pi^2}B^2\right) \tag{24a}$$

$$h_b = \pi^3\left(8\pi A^2 + \tfrac{16}{3}AB + \tfrac{1}{2}\pi B^2\right) \tag{24b}$$

$$h_s = \pi\left(4\pi A^2 + \tfrac{32}{3}AB + (\tfrac{1}{2}\pi+1)B^2\right) \tag{24c}$$

$$h_T = \frac{1}{2}(C_1^2+C_2^2) + (-2A+(\frac{4}{\pi}-2)B)(C_1+C_2) + 4A^2 + (8-\frac{16}{\pi})AB + (5-\frac{14}{\pi})B^2 \tag{24d}$$

Substituting Eq. (24) into Eq. (22), we have

$$\overline{\sigma}_{c,S} = \frac{\left(\begin{array}{l} \frac{\pi^2\kappa V_m}{3\rho^2}\left(2\pi A^2 + \frac{4}{3}AB + \frac{1}{8}\pi B^2\right) + \frac{1}{2(1-V_m)(1+v_p)}\left(2\pi A^2 + \frac{16}{3}AB + \left(\frac{1}{4}\pi+\frac{1}{2}\right)B^2\right) \\ + \frac{\rho^2 V_m^2}{\pi(1-V_m)(1-v_p{}^2)}\left(\frac{1}{2}(C_1^2+C_2^2) + \left(-2A+\left(\frac{4}{\pi}-2\right)B\right)(C_1+C_2) + 4A^2 + \left(8-\frac{16}{\pi}\right)AB + \left(5-\frac{14}{\pi}\right)B^2\right) \end{array}\right)}{\left(2\pi A^2 + \frac{16}{3}AB + \frac{1}{2}\pi B^2\right) - 2\pi\left(8\pi\frac{(\gamma^2+3\pi^2)-2\pi\gamma\coth(\gamma/4)}{(\gamma^2+\pi^2)(\gamma^2+9\pi^2)}AB + \frac{\gamma\coth(\gamma/4)}{\gamma^2+4\pi^2}B^2\right)} \tag{25}$$

For the critical load of the lowest buckling mode, there should be

$$\begin{cases} \frac{\partial\overline{\sigma}_{c,S}}{\partial C_1} = 0 \\ \frac{\partial\overline{\sigma}_{c,S}}{\partial C_2} = 0 \end{cases} \tag{26a}$$

and

$$\begin{cases} \frac{\partial\overline{\sigma}_{c,S}}{\partial A} = 0 \\ \frac{\partial\overline{\sigma}_{c,S}}{\partial B} = 0 \end{cases} \tag{26b}$$

We first apply Eq. (26a). By substituting Eq. (25) into Eq. (26a), we obtain

$$C_1 = C_2 = 2A + \left(2-\frac{4}{\pi}\right)B \tag{27}$$

Substituting Eq. (27) into Eq. (25), we have

$$\overline{\sigma}_{c,S} = \frac{N}{D} \tag{28}$$

where

$$\begin{aligned} N &= \frac{\pi^2\kappa V_m}{3\rho^2}\left(2\pi A^2 + \frac{4}{3}AB + \frac{1}{8}\pi B^2\right) + \frac{1}{2(1-V_m)(1+v_p)}\left(2\pi A^2 + \frac{16}{3}AB + \left(\frac{1}{4}\pi+\frac{1}{2}\right)B^2\right) \\ &\quad + \frac{\rho^2 V_m^2}{\pi(1-V_m)(1-v_p^2)}\left(1+\frac{2}{\pi}-\frac{16}{\pi^2}\right)B^2 \\ D &= \left(2\pi A^2 + \frac{16}{3}AB + \frac{1}{2}\pi B^2\right) - 2\pi\left(8\pi\frac{(\gamma^2+3\pi^2)-2\pi\gamma\coth(\gamma/4)}{(\gamma^2+\pi^2)(\gamma^2+9\pi^2)}AB + \frac{\gamma\coth(\gamma/4)}{\gamma^2+4\pi^2}B^2\right) \end{aligned} \tag{29}$$

Then substituting Eq. (28) into Eq. (26b), we have

$$\begin{bmatrix} a_1-\overline{\sigma}_{c,S}b_1 & a_2-\overline{\sigma}_{c,S}b_2 \\ a_3-\overline{\sigma}_{c,S}b_3 & a_4-\overline{\sigma}_{c,S}b_4 \end{bmatrix}\begin{pmatrix} A \\ B \end{pmatrix} = 0 \tag{30}$$

where

$$a_1 = \frac{4\pi^3\kappa V_m}{3\rho^2} + \frac{2\pi}{(1-V_m)(1+v_p)}$$

$$a_2 = \frac{4\pi^2\kappa V_m}{9\rho^2} + \frac{8}{3(1-V_m)(1+v_p)}$$

$$a_3=\frac{4\pi^2\kappa V_m}{9\rho^2}+\frac{8}{3(1-V_m)(1+\nu_p)}$$
$$a_4=\frac{\pi^3\kappa V_m}{12\rho^2}+\frac{\pi+2}{4(1-V_m)(1+\nu_p)}+\frac{2\rho^2V_m^2}{\pi(1-V_m)(1-\nu_p^2)}\left(1+\frac{2}{\pi}-\frac{16}{\pi^2}\right) \tag{31a}$$

and

$$b_1=4\pi$$
$$b_2=\frac{16}{3}-16\pi^2\frac{(\gamma^2+3\pi^2)-2\pi\gamma\coth(\gamma/4)}{(\gamma^2+\pi^2)(\gamma^2+9\pi^2)}$$
$$b_3=\frac{16}{3}-16\pi^2\frac{(\gamma^2+3\pi^2)-2\pi\gamma\coth(\gamma/4)}{(\gamma^2+\pi^2)(\gamma^2+9\pi^2)}$$
$$b_4=\pi-\frac{4\pi\gamma\coth(\gamma/4)}{\gamma^2+4\pi^2} \tag{31b}$$

The criterion for non-zero solution of Eq. (30) is

$$\det\left(\begin{bmatrix}a_1-\overline{\sigma}_{c,S}b_1 & a_2-\overline{\sigma}_{c,S}b_2\\ a_3-\overline{\sigma}_{c,S}b_3 & a_4-\overline{\sigma}_{c,S}b_4\end{bmatrix}\right)=0 \tag{32}$$

by which we obtain the expression of the normalized critical buckling load as

$$\overline{\sigma}_{c,S}=\frac{(a_1b_4+a_4b_1-a_2b_3-a_3b_2)-\sqrt{(a_1b_4+a_4b_1-a_2b_3-a_3b_2)^2-4(b_1b_4-b_2b_3)(a_1a_4-a_2a_3)}}{2(b_1b_4-b_2b_3)} \tag{33}$$

If we further define

$$\overline{B}=\frac{B}{A}=-\frac{a_1-\overline{\sigma}_{c,S}b_1}{a_2-\overline{\sigma}_{c,S}b_2} \tag{34}$$

and substitute Eq. (34) back to Eq. (25) (note that $\overline{B}$ is already known), we get an alternative expression of the normalized critical buckling force as

$$\overline{\sigma}_{c,S}=\frac{\pi^2\kappa V_m}{3\rho^2}\eta_1(\overline{B})+\frac{1}{2(1-V_m)(1+\nu_p)}\eta_2(\overline{B})+\frac{\rho^2V_m^2}{\pi(1-V_m)(1-\nu_p{}^2)}\eta_3(\overline{B}) \tag{35}$$

where

$$\begin{cases}\eta_1(\overline{B})=\frac{1}{\overline{D}}\left(2\pi+\frac{4}{3}\overline{B}+\frac{1}{8}\pi\overline{B}^2\right)\\ \eta_2(\overline{B})=\frac{1}{\overline{D}}\left(2\pi+\frac{16}{3}\overline{B}+(\frac{1}{4}\pi+\frac{1}{2})\overline{B}^2\right)\\ \eta_3(\overline{B})=\frac{1}{\overline{D}}(1+\frac{2}{\pi}-\frac{16}{\pi^2})\overline{B}^2\\ \overline{D}=\left(2\pi+\frac{16}{3}\overline{B}+\frac{1}{2}\pi\overline{B}^2\right)-2\pi\left(8\pi\frac{(\gamma^2+3\pi^2)-2\pi\gamma\coth(\gamma/4)}{(\gamma^2+\pi^2)(\gamma^2+9\pi^2)}\overline{B}+\frac{\gamma\coth(\gamma/4)}{\gamma^2+4\pi^2}\overline{B}^2\right)\end{cases} \tag{36}$$

We can see that the three terms in Eq. (35) have clear physical implication. The first term is coming from the bending energy of mineral, the second term is from the shear deformation energy of protein, and the third term is from the tension deformation energy of protein. This result indicated that the release of the membrane energy is balanced by the increase of the bending energy of mineral, and the changing of the shear energy and tension energy of the protein matrix.

4.2.2. Anti-symmetric buckling mode

Similarly, based on the initial perturbation solution of the buckling mode Eqs. (S17) and (S5) and numerical simulation results (Section S.3 and Fig. S2 in Supporting information), we assume the anti-symmetric buckling mode of minerals $A'B'$ and $C'D'$ (see Fig. 6) as

$$\begin{cases}\tilde{v}_1(\xi)=A\cos2\pi\xi+B(\xi+\frac{1}{4})\\ \tilde{v}_2(\xi)=A\cos2\pi\xi-B(\xi-\frac{1}{4})\end{cases} \tag{37}$$

Substituting Eq. (37) into Eq. (20), we have

$$h_m=2\pi^2A^2+B^2+\frac{16\pi\gamma\coth(\gamma/4)}{\gamma^2+4\pi^2}AB \tag{38a}$$

$$h_b=8\pi^4A^2 \tag{38b}$$

$$h_s=4\pi^2A^2 \tag{38c}$$

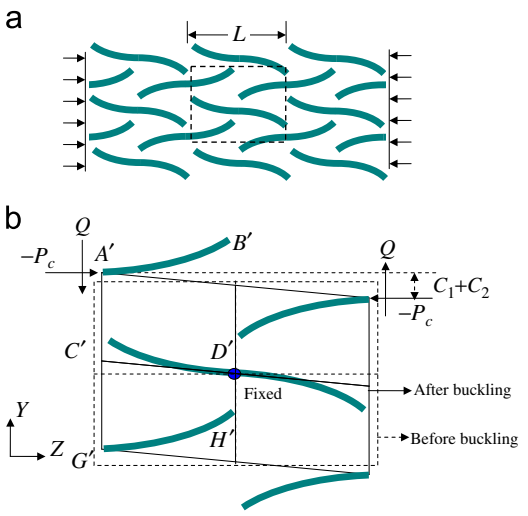

Fig. 6. Illustration of the anti-symmetric mode of local buckling of mineral in the nanocomposite structure. (a) Buckling deformation pattern in a periodic manner; (b) illustration of equilibrium analysis of minerals under the axial loading in one periodic structure unit.

$$h_T = \tfrac{1}{2}(C_1^2+C_2^2)+\tfrac{1}{12}B^2 \tag{38d}$$

Then substituting Eq. (38) into Eq. (22) results in

$$\overline{\sigma}_{c,A} = \frac{\frac{\pi^2\kappa V_m}{3\rho^2}2\pi^2A^2 + \frac{1}{2(1-V_m)(1+\nu_p)}2\pi^2A^2 + \frac{\rho^2V_m^2}{\pi(1-V_m)(1-\nu_p^2)}(\frac{\pi}{2}(C_1^2+C_2^2)+\frac{\pi}{12}B^2)}{2\pi^2A^2+B^2+\frac{16\pi\gamma\coth(\gamma/4)}{\gamma^2+4\pi^2}AB} \tag{39}$$

To derive the lowest critical buckling force, we first use Eq. (26a) to determine the value of C_1 and C_2. Substituting Eq. (39) into Eq. (26a) immediately results in

$$C_1 = C_2 = 0 \tag{40}$$

Substituting Eq. (40) into Eq. (39), we have

$$\overline{\sigma}_{c,A} = \frac{N}{D} \tag{41}$$

where

$$N = \frac{\pi^2\kappa V_m}{3\rho^2}2\pi^2A^2 + \frac{1}{2(1-V_m)(1+\nu_p)}2\pi^2A^2 + \frac{\rho^2V_m^2}{\pi(1-V_m)(1-\nu_p^2)}\frac{\pi}{12}B^2$$
$$D = 2\pi^2A^2+B^2+\frac{16\pi\gamma\coth(\gamma/4)}{\gamma^2+4\pi^2}AB \tag{42}$$

Then substituting Eq. (41) into Eq. (26b), we have

$$\begin{bmatrix} a_1-\overline{\sigma}_{c,A}b_1 & a_2-\overline{\sigma}_{c,A}b_2 \\ a_3-\overline{\sigma}_{c,A}b_3 & a_4-\overline{\sigma}_{c,A}b_4 \end{bmatrix}\begin{pmatrix} A \\ B \end{pmatrix} = 0 \tag{43}$$

where

$$a_1 = \frac{4\pi^4\kappa V_m}{3\rho^2}+\frac{2\pi^2}{(1-V_m)(1+\nu_p)}$$
$$a_2 = 0$$
$$a_3 = 0$$
$$a_4 = \frac{\rho^2V_m^2}{6(1-V_m)(1-\nu_p^2)} \tag{44a}$$

and

$$b_1 = 4\pi^2$$
$$b_2 = \frac{16\pi\gamma\coth(\gamma/4)}{\gamma^2+4\pi^2}$$
$$b_3 = \frac{16\pi\gamma\coth(\gamma/4)}{\gamma^2+4\pi^2}$$

$$b_4 = 2 \tag{44b}$$

Applying the criterion of nonzero solution to Eq. (43), we have

$$\det\left(\begin{bmatrix} a_1-\overline{\sigma}_{c,A}b_1 & a_2-\overline{\sigma}_{c,A}b_2 \\ a_3-\overline{\sigma}_{c,A}b_3 & a_4-\overline{\sigma}_{c,A}b_4 \end{bmatrix}\right) = 0 \tag{45}$$

which results in

$$\overline{\sigma}_{c,A} = \frac{(a_1b_4+a_4b_1-a_2b_3-a_3b_2)-\sqrt{(a_1b_4+a_4b_1-a_2b_3-a_3b_2)^2-4(b_1b_4-b_2b_3)(a_1a_4-a_2a_3)}}{2(b_1b_4-b_2b_3)} \tag{46}$$

Similarly, if we define

$$\overline{B} = \frac{B}{A} = -\frac{a_1-\overline{\sigma}_{c,A}b_1}{a_2-\overline{\sigma}_{c,A}b_2} \tag{47}$$

and substitute Eq. (47) back to Eq. (39), we obtain

$$\overline{\sigma}_{c,A} = \frac{\pi^2\kappa V_m}{3\rho^2}\eta_1(\overline{B}) + \frac{1}{2(1-V_m)(1+\nu_p)}\eta_2(\overline{B}) + \frac{\rho^2V_m^2}{\pi(1-V_m)(1-\nu_p{}^2)}\eta_3(\overline{B}) \tag{48}$$

where

$$\begin{cases} \eta_1(\overline{B}) = \frac{2\pi^2}{\overline{D}}, \quad \eta_2(\overline{B}) = \frac{2\pi^2}{\overline{D}}, \quad \eta_3(\overline{B}) = \frac{\pi\overline{B}^2}{12\overline{D}} \\ \overline{D} = 2\pi^2 + \overline{B}^2 + \frac{16\pi\gamma}{\gamma^2+4\pi^2}\coth(\gamma/4)\overline{B} \end{cases} \tag{49}$$

Again, we can see that the first, second and third terms of Eq. (48) are coming from the bending energy of mineral, the shear energy and the tension energy of protein, respectively.

5. Results and discussion

5.1. Effect of the aspect ratio on the buckling strength

The expressions of buckling strength of the symmetric and anti-symmetric modes of the nanocomposite structure are given in Eqs. (35) and (48), respectively. The comparison between these two buckling modes is illustrated in Fig. 7. As we can see, the buckling strength of the symmetric mode is higher than that of the anti-symmetric mode at small aspect ratio, while it becomes lower when the aspect ratio is larger than a critical value (e.g., around 12 for V_m=45% in the case of bone and around 6 for V_m=95% in the case of nacre). That is, the anti-symmetric mode is dominant at small aspect ratio, while the symmetric mode is dominant at comparatively large aspect ratio. However, the buckling strength of these two modes asymptotically approaches to each other when the aspect ratio becomes extremely large.

It is noteworthy that in the above results, the volume fraction of mineral, such as 45% and 95% we chose for the nanocomposite structures (the lowest level) of bone and shell, respectively, are approximate estimations according to experimental observations, and may change in a range for different species. For example, for the nanocomposite structure in mineralized fibrils of bone, the mineral content was estimated around 43% (Fratzl et al., 2004); for the nanostructure of shell, volume fraction of mineral is 90–95.5% (Wang et al., 2001; Kamat et al., 2000). The volume fraction of higher hierarchical levels should be larger according to references (Fratzl et al., 2004; Zhang et al., 2011).

To gain more insights into the effect of the aspect ratio, the buckling strength of the nanocomposite structure is compared with that of the ideally continuous-fiber reinforced composite which is given by Rosen's (1964) model as

$$\overline{\sigma}_c^{RS} = \frac{1}{2(1+\nu_p)(1-V_m)} + \frac{m^2\pi^2V_m\kappa}{3\rho_G^2} \tag{50}$$

where ρ_G=L_G/H_m (L_G is the global length of continuous fibers, see Fig. 8), V_m and κ are global aspect ratio, volume fraction and modulus ratio, respectively (m in Eq. (50) is equal to 1 for the non-dilute fiber reinforced composites. The composites may adopt the higher order modes with larger wave number, i.e., $m>1$, only for the dilute ones (Parnes and Chiskis, 2002)). Fig. 7 shows that the buckling strength of the nanocomposite structures asymptotically approaches to that of Rosen's model as the aspect ratio ρ increases. This can be proved by checking the evolution of buckling modes with the increase of the aspect ratio as shown in Fig. 9. At the small aspect ratio, the buckling modes of the nanocomposite structure (the symmetric and anti-symmetric) are neither pure shear mode nor pure tension mode. But as the aspect ratio increases, both of the two modes approach to the shear mode of Rosen's model. For the sake of convenience of analysis, here we define the first critical aspect ratio at which the $\overline{\sigma}_{c,S} > \overline{\sigma}_{c,A}$ as $\rho_{c,1}$ in Fig. 7, and define a second critical aspect ratio as $\rho_{c,2}$ at which the buckling strength of the two modes approaches that of Rosen's model which given by the criterion

$$\sqrt{(\overline{\sigma}_{c,S}-\overline{\sigma}_c^{RS})^2+(\overline{\sigma}_{c,A}-\overline{\sigma}_c^{Rs})^2}\Big/\overline{\sigma}_c^{RS} < 1\% \tag{51}$$

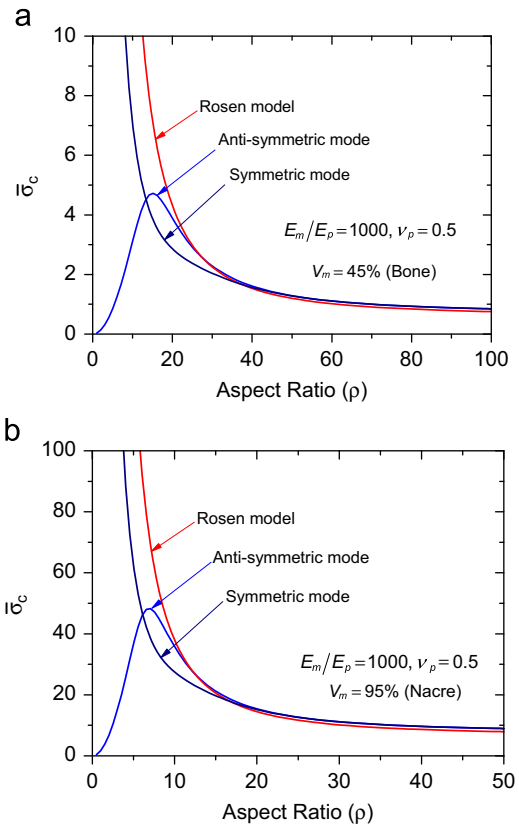

Fig. 7. Buckling strength of the symmetric and anti-symmetric modes of the nanocomposite structure in comparison with that of the continuous-fiber reinforced composite predicted by Rosen's model at different aspect ratio of mineral. (a) Volume fraction of mineral being equal to 45% in the case of bone. (b) Volume fraction of mineral being equal to 95% in the case of nacre.

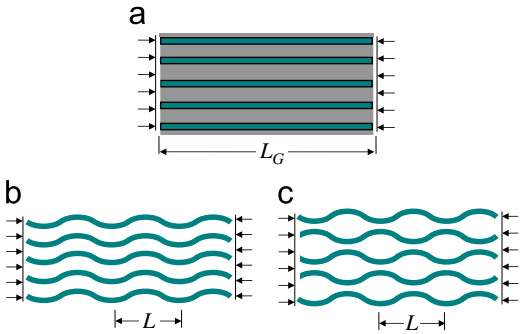

Fig. 8. Local buckling modes of the continuous-fiber reinforced composite. (a) The shear mode and (b) the tension mode (transverse mode).

The differences in the buckling strength between the biological nanocomposite structure and the ideally continuous-fiber reinforced composite can be understood by a comparison of their microstructures (see Figs. 2a and 8a) as follows. Imagining each two neighboring mineral crystals in longitudinal direction were welded together at their adjacent tips, the nanocomposite would become the continuous nanofiber reinforced composites. Therefore, from this point of view, the nanocomposite structure is "imperfect" structure in comparison with the continuous-fiber reinforce composite. The crack-like flaws at the tip zones between neighboring minerals will weaken the buckling strength of the nanocomposite in comparison with the flaw-free continuous fibers reinforced composites (Fig. 7). However, it is very difficult to fabricate the ideally continuous fibers in the practical applications, therefore how to optimize the strength of the composites with the discontinuous reinforcement is a challenging problem.

This study showed that the natural biological materials may have found a solution of solving above problem. According to our analysis, the staggered alignment of mineral crystals takes important roles in the structural stability of the nanocomposite structure. Although the crack-like tip zones may weaken the buckling strength, the effect of this

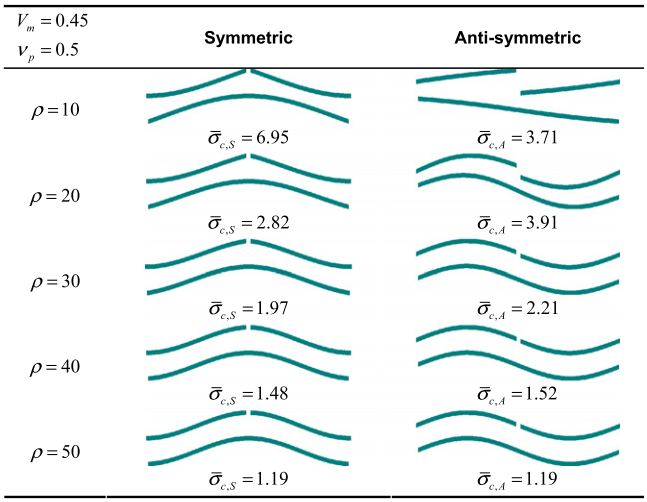

Fig. 9. Evolution of the symmetric and anti-symmetric modes of the nanocomposite structure as a function of aspect ratio of mineral, showing that the two buckling modes approach to the shear mode of the continuous-fiber reinforce composites as the aspect ratio increases.

imperfection can be largely eliminated by increasing the aspect ratio of mineral crystals with the help of their staggered alignment. This staggered arrangement allows the buckling strength of the discontinuous mineral reinforced composite to approach to that of the continuous-fiber reinforced composite when the aspect ratio of the mineral is increased to a threshold value, as shown in Figs. 7 and 9. For example, for bone, the buckling strength of the nanocomposite structure can reach that of Rosen's model at an aspect ratio of 40, while for the nacre, the buckling strength can reach that of Rosen's model at an aspect ratio of 18. These results imply that the buckling strength becomes insensitive to the flaws (the crack-like tip zones) at large aspect ratio.

To justify the assumption of traction free condition at mineral tips in our theoretical model, we double-checked the value of relative displacement between the tips of neighboring minerals at the critical loading of buckling. The results showed that it is much smaller than the size of tip zone for bone, i.e,, the mineral tips will never contact with each other before buckling and therefore the traction free condition should be satisfied. But for shell, we found that there is possibility of contact before buckling for relative small aspect ratio. Because this study is focused on the buckling behaviors at large aspect ratio, the non-contacting assumption of the tips should be applicable.

5.2. Local buckling versus global buckling

This study has been focused on the local buckling of nanocomposites by assuming that the minerals buckle within the periodic nanocomposite structure. However, in practical, whether local or global buckling will happen in the nanocomposite depends on the aspect ratio of the mineral. Here we will make a discussion about the relationship between the local buckling and the global buckling.

According to the preceding sections, Eqs. (35) and (48) give the local buckling strength of the symmetric and anti-symmetric modes, respectively, while Eq. (50) gives the global buckling strength. When the nanocomposite performs global buckling, because $\rho_G \to \infty$ and $\rho \to \infty$, Eq. (50) degenerates to

$$\bar{\sigma}_{c,L} = \frac{1}{2(1+\nu_p)(1-V_m)} \tag{52}$$

which sets the lower limit of Rosen's model. There is a cross point between this lower limit and the buckling strength curve of the anti-symmetric mode as depicted in Fig. 10. We define the corresponding aspect ratio of this point as $\rho_{c,0}$ below which the local buckling strength is lower than the global buckling strength. Therefore, we can predict that once the aspect ratio is lower than $\rho_{c,0}$, the nanocomposite will have local buckling. However, when the aspect ratio is larger than $\rho_{c,2}$, the nanocomposite will have global buckling. When $\rho_{c,0} < \rho < \rho_{c,2}$, the nanostructure may exhibit a mixed buckling mode.

These results suggest a mechanism of buckling mode transition from the local to global buckling behaviors of biological nanocomposites. We showed that the aspect ratio of mineral can regulate the coordination among minerals with staggered alignment. Through this regulation, the buckling strength exhibits a biphasic dependence on the aspect ratio which enables the local to global buckling transition.

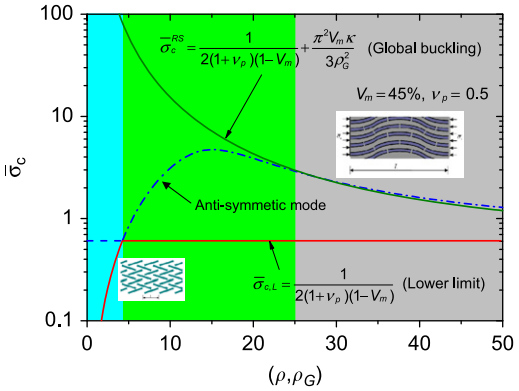

Fig. 10. Illustration of the competition between the local buckling mode and the global buckling mode of the nanocomposite structure as a function of aspect ratio.

5.3. *Effect of the volume fraction*

Besides the aspect ratio, the volume fraction of mineral also influences the buckling strength of the two modes of nanocomposites and their relationship with Rosen's shear mode. Fig. 11 shows that increasing of the volume fraction of mineral significantly increases the buckling strength of these two modes, suggesting that large volume fraction can effectively restrict deformation of mineral crystals and protein matrix. In addition, the difference in the buckling strength between the nanocomposite structure and that of Rosen's model decreases with the increase of the volume fraction, which indicates that the flaw-like imperfection caused by the tip zones are compensated by the large volume fraction. Furthermore, we found that the volume fraction of mineral would influence the competition between the symmetric mode and the anti-symmetric mode. For instance, Fig. 12 depicts the variation of $\rho_{c,1}$ and $\rho_{c,2}$ as the function of the volume fraction. We can see that both of the two critical aspect ratio values decrease as the increase of the volume fraction, and the value of $\rho_{c,1}$ reduces much faster at the low volume fraction region than it does at the high volume fraction region, as shown in Fig. 12. This result implies that a high volume fraction will allow the strength of the anti-symmetric mode to be larger than that of the symmetric model at a comparatively small aspect ratio. In addition, the high volume fraction allows the buckling strength of the two modes to approach that of Rosen's model at small aspect ratio.

We also can see that there is a lower limit of $\rho_{c,1}$ ($\rho_{c,1}^L$) value below which the buckling strength of the anti-symmetric mode is always lower than that of the symmetric mode for different volume fraction of mineral (see Fig. 12), and there is an upper limit of $\rho_{c,1}$ ($\rho_{c,1}^H$) value beyond which the buckling strength of the anti-symmetric mode is always higher than that of the symmetric mode (see Fig. 12). Similarly, there is also a lower limit of $\rho_{c,2}$ ($\rho_{c,2}^L$) value below which the buckling strength of the two modes of the nanocomposite structure will never approach that of the Rosen mode by changing the volume fraction, and there is an upper limit of $\rho_{c,2}$ ($\rho_{c,2}^H$) value beyond which the buckling strength of the two modes will always approach to that of the Rosen mode at different volume fraction.

5.4. *Effect of the hierarchical structures*

Previous studies showed that the hierarchical structures can effectively enhance the stiffness and fracture toughness of biological nanocomposites (Gao, 2006). In this section, we discuss the roles of hierarchical structure on the buckling strength of these materials. According to the preceding discussion, the nanocomposites with large aspect ratio of mineral crystals would perform global buckling with buckling strength given by Eq. (52) because the minerals behave like long and continuous fibers. As we can see, the global buckling strength of the nanocomposite structure does not depend on the elastic properties of mineral, but only depends on its volume fraction. If the total volume fraction of mineral is constant, the structural hierarchy will effectively increase the volume fraction of hard phase in each level of hierarchy (note that for the higher level, the hard phase itself will be the composite of mineral and protein). For example, for a self-similar hierarchical structure depicted by the inset in Fig. 13, there is

$$V_{m,T} = \prod_{n=1}^{N} V_{m(n)} \tag{53}$$

where $V_{m,T}$ is the total volume fraction of the hierarchical structure and $V_{m(n)}$ is the volume fraction of hard phase in the nth level. For the nth level of hierarchical structure, there is,

$$V_{m(n)} = V_{m,T}^{1/N} \tag{54}$$

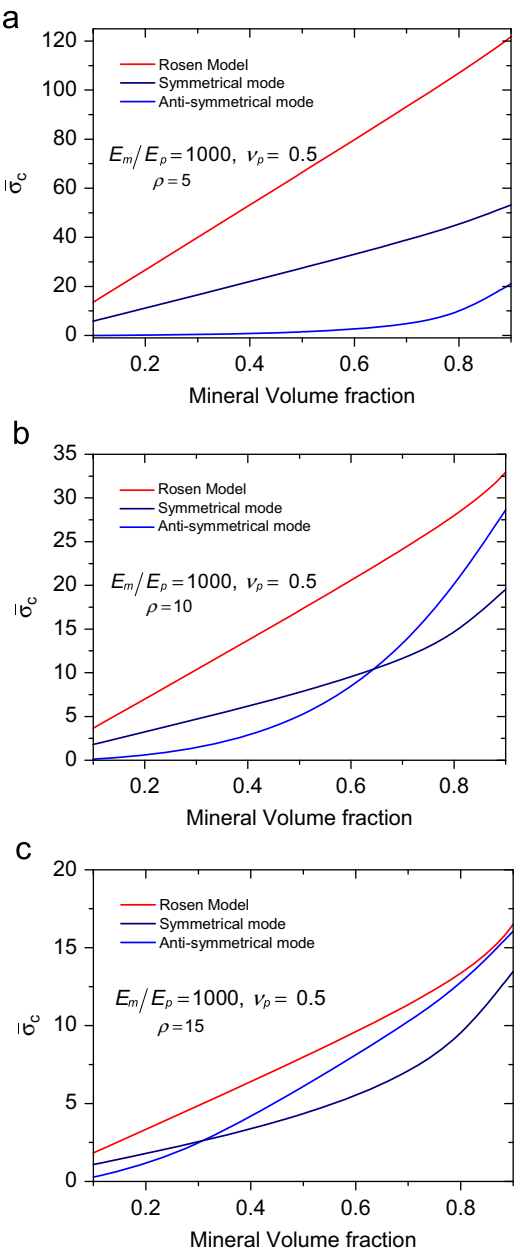

Fig. 11. Buckling strength of the symmetric and the anti-symmetric modes of the nanocomposite structure in comparison with that of the continuous-fiber reinforced composite predicted by Rosen's model at different volume fraction of mineral. (a) $\rho=5$; (b) $\rho=10$ and (c) $\rho=15$.

Substituting Eq. (54) into Eq. (52), we obtain

$$\overline{\sigma}_{c(n)}=\frac{1}{2(1+\nu_p)(1-V_{m,T}^{1/N})} \tag{55}$$

It has been checked that the second term in Eq. (50) is always negligible at each level of the hierarchy. We can see that the buckling strength of biological materials can be effectively increased by simply increasing the number of levels of the hierarchy. Note that the materials have the same buckling strength at each level of their hierarchy, and the buckling strength increases with the increase of the number of levels in the hierarchy, as shown in Fig. 13. Different from the tensile strength of the hierarchical structures that degenerates with the increase of the levels of hierarchy (Gao, 2006), the buckling strength is uniformly increased at all levels of the hierarchy. This feature is remarkably crucial for the functions of biological materials, such as bone and nacre, which principally sustain the compressive load.

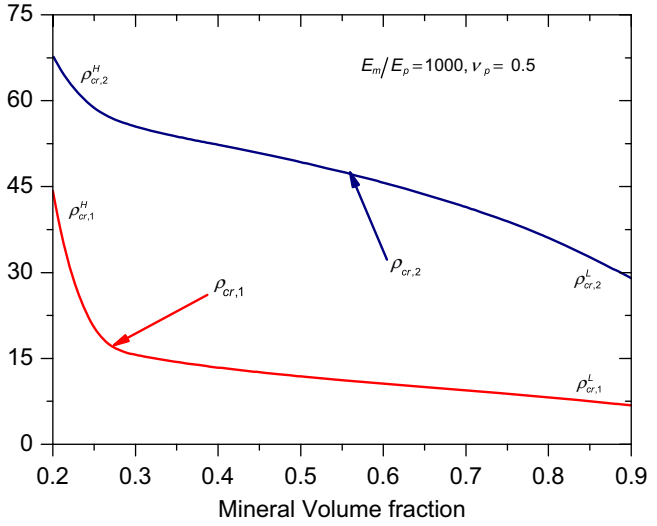

Fig. 12. The variation of the two critical aspect ratio $\rho_{c,1}$ and $\rho_{c,2}$ as the functions of the volume fraction of mineral.

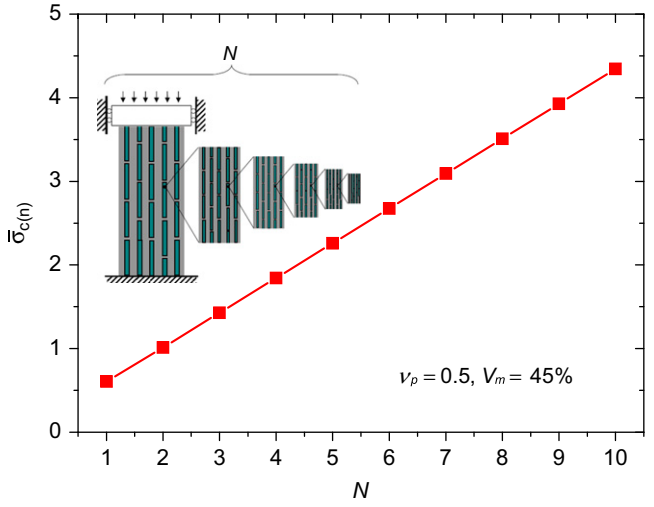

Fig. 13. Effect of the number of levels of hierarchy on the buckling strength of the self-similar hierarchical composite structure.

Note that this effect of the hierarchical structure is closely related to the results of local buckling analysis. It was shown that when the aspect ratio of mineral is small, the nanocomposite will perform local buckling; however, with the increase of the aspect ratio to a critical value, the nanocomposite will have a mode transition from the local buckling to a global buckling behavior, insensitive to the existing defects (tip zones between mineral crystals); therefore it achieves the buckling strength of ideally continuous fiber reinforced composites, i.e., global buckling behavior. With this property of buckling, the biological materials can achieve global buckling at macroscopic scales through equally distributing buckling strength among different levels of hierarchy and therefore avoiding local buckling at low levels of hierarchy, which allows the biological materials to achieve optimum buckling strength. The local buckling analysis also provided the critical values of aspect ratio of the hard phase in each hierarchical level.

On the other hand, if the nanocomposite structure can not achieve the transition from the local to global buckling, e.g., because of small aspect ratio, then the local buckling will happen, and this localization of deformation might propagate to higher levels of hierarchy, which will largely decrease the buckling strength of high levels. However, the systematic analysis of the propagation of buckling localization among different hierarchical levels will be another complex problem and beyond the scope of this study.

5.5. Further discussion with previous studies

Compared with existing studies, the scientific questions explored in the present work are different. We are interested in the effect of the unique microstructures of biological materials on their micro-buckling behaviors, particularly, the roles of the staggered alignment of minerals and their coordination in the buckling behaviors as well as the effects of the structure hierarchy on the buckling strength. As a result, our mechanical model and predictions are also different from those of prior studies.

Firstly, this study is different from the previous work (Ji et al., 2004). That work only studied a SINGLE mineral, and it did not consider the coordination of this mineral with its neighboring minerals by adopting a strong assumption that the neighboring minerals were rigid without deformation, which resulted in the buckling strength of a high order buckling mode of the nanocomposite structure.

In comparison, the present study studied MULTIPLE minerals by focusing on the effect of coordination among these minerals when they perform buckling deformation. Therefore, this study is significantly different from Ji et al. (2004) in both the mechanics of buckling behaviors and the method and difficulty of mathematical analysis. For example, our results showed that different from the single mineral, the multiple minerals have more complex buckling behaviors. For instance, they have two different buckling modes because of the coordination, i.e., the symmetric mode and anti-symmetric mode. There is a critical value of aspect ratio. When the aspect ratio is smaller than this critical value, the minerals will perform anti-symmetric mode, while when the aspect ratio is larger than the critical value, they will perform symmetric mode. Therefore, there is a biphasic dependence of the buckling strength on the aspect ratio of mineral, i.e., at small aspect ratio, the buckling strength is increasing with the increase of aspect ratio, but at large aspect ratio, the buckling strength is decreasing with the increase of the aspect ratio. This behavior of multiple minerals is new and distinct from that of single mineral.

Secondly, this study is also different from the work by Rosen (1964). That work studied the buckling behavior of ideally continuous fiber reinforced composite. Therefore, the predictions of Rosen model are not applicable to the nanocomposite structure of biological materials with staggered alignment of minerals in protein matrix and discontinuity (gap) between the minerals. It was shown that the buckling strength predicted by Rosen model is larger than that of the nanocomposite structure, and monotonically decreases with the increase of the aspect ratio of mineral, which is very different from the biphasic dependence of buckling strength of the nanocomposite structure with respect to the aspect ratio.

Thirdly, the effect of the hierarchical structure on buckling strength has not been studied before. We found that the hierarchical structure play important roles in the buckling behavior of biological nanocomposites. We showed that with the help of large aspect ratio, the local buckling can be suppressed at all levels of hierarchy, and achieve an equally distributed buckling strength at each level. This novel property will enable the biological nanocomposites to achieve global buckling at macroscopic scales by avoiding local buckling through hierarchical design. This finding is critically important for the design of the bio-inspired novel composite materials with multiple levels of hierarchy.

6. Conclusions

This paper presents an analytical analysis of the buckling behaviors of biological nanocomposites, aimed to find mechanical principles by which nature designs nanocomposites with high elastic stability. The unique geometry and staggered arrangement of mineral crystals in the nanocomposite structure were explicitly considered in the theoretical model. Despite of the structural complexity of the model, analytical solutions of the buckling strength were obtained by solving the problem using a combination of the perturbation method and the energy method. Two local buckling modes, i.e., the symmetric and anti-symmetric modes, were analyzed. The effect of the geometry, staggered arrangement and volume fraction of mineral crystals as well as the structural hierarchy on the buckling behaviors of biological nanocomposites were studied. The main findings of this study are summarized as follows.

The aspect ratio of minerals plays an important role in the buckling behaviors of the nanocomposite structure. When the aspect ratio is small, the buckling strength of the anti-symmetric mode is lower than that of the symmetric mode, while when the aspect ratio increases to a critical value $\rho_{c,1}$ the buckling strength of the anti-symmetric mode becomes larger than that of the symmetric mode. This property makes the buckling strength of the nanocomposites exhibit a biphasic dependence on the aspect ratio. Furthermore, the buckling strength of these two modes of the nanocomposite structure can approach to that of Rosen's model when the aspect ratio increases to a second threshold value $\rho_{c,2}$ with help of the staggered alignment of minerals. This implies that the buckling strength becomes insensitive to the existing flaws at large aspect ratio, as the large aspect ratio compensates the weakening effects of the tip zones, which might explain why the mineral crystals in biological nanocomposites always have large aspect ratio.

Further analyses suggest that once the aspect ratio is lower than the threshold value $\rho_{c,0}$, the nanocomposite structure will have local buckling as shown in Fig. 10. In contrast, when the aspect ratio is larger than $\rho_{c,2}$, the nanocomposite will have global buckling mode. When $\rho_{c,0} < \rho < \rho_{c,2}$, the nanostructure might have mixed buckling mode depending on the ratio of L_G/L. These results suggested that the aspect ratio of mineral can regulate the coordination among minerals with staggered alignment. Through this regulation, the buckling strength exhibits a biphasic dependence on the aspect ratio which enables the local to global buckling transition.

The volume fraction of mineral also plays important roles. Increasing the volume fraction can significantly enhance the structural stability of the nanocomposite. The mechanism behind is that the large volume fraction will restrict the deformation of minerals as well as that of protein matrix. It was shown that with the increase of the volume fraction, the difference in buckling strength between the nanocomposite structure and Rosen's model decreases, which indicates that the effect of flaw-like tip zones between minerals are compensated by the large volume fraction. This result might suggest that biological materials with large volume fraction of mineral are likely to have evolved to adapt to high compressive load experienced by the animals such as nacre under the deep sea water.

In addition, we found that the hierarchical structure design can effectively improve the buckling strength of biological materials. We showed that with the help of large aspect ratio, the local buckling can be suppressed at all levels of hierarchy, and achieve an equally distributed buckling strength at each level. This property will enable the biological nanocomposites achieve global buckling at macroscopic scales by avoiding local buckling through hierarchical design. More remarkably, different from the tensile strength that degenerates with the increase of the levels of hierarchy, the buckling strength will be uniformly increased at all the levels of the hierarchy. This point is critically important for the design of the bio-inspired novel composite materials with multiple levels of hierarchy.

Acknowledgment

This research was supported from the National Natural Science Foundation of China through Grant nos. 10732050, 10872115, and 11025208.

Appendix A. Supporting information

Supplementary data associated with this article can be found in the online version at http://dx.doi.org/10.1016/j.jmps.2012.05.003.

References

Bonderer, L.J., Studart, A.R., Gauckler, L.J., 2008. Bioinspired design and assembly of platelet reinforced polymer films. Science 319 (5866), 1069–1073.
Currey, J.D., 1977. Mechanical-properties of mother of pearl in tension. Proc. R. Soc. London Ser. B—Biol. Sci. 196 (1125), 443.
Dashkovskiy, S., Suhr, B., Tushtev, K., Grathwohl, G., 2007. Nacre properties in the elastic range: influence of matrix incompressibility. Comput. Mater. Sci. 41 (1), 96–106.
Fang, L.M., Gao, P., Leng, Y., 2007. High strength and bioactive hydroxyapatite nano-particles reinforced ultrahigh molecular weight polyethylene. Compos. Part B—Eng. 38 (3), 345–351.
Fratzl, P., Gupta, H.S., Paschalis, E.P., Roschger, P., 2004. Structure and mechanical quality of the collagen–mineral nano-composite in bone. J. Mater. Chem. 14 (14), 2115–2123.
Fratzl, P., Weinkamer, R., 2007. Nature's hierarchical materials. Prog. Mater. Sci. 52 (8), 1263–1334.
Gao, H., 2006. Application of fracture mechanics concepts to hierarchical biomechanics of bone and bone-like materials. Int. J. Fract. 138 (1–4), 101–137.
Gao, H.J., Ji, B.H., Jager, I.L., Arzt, E., Fratzl, P., 2003. Materials become insensitive to flaws at nanoscale: lessons from nature. Proc. Natl. Acad. Sci. USA 100 (10), 5597–5600.
Gupta, H.S., Seto, J., Wagermaier, W., Zaslansky, P., Boesecke, P., Fratzl, P., 2006. Cooperative deformation of mineral and collagen in bone at the nanoscale. Proc. Natl. Acad. Sci. USA 103 (47), 17741–17746.
Gupta, H.S., Wagermaier, W., Zickler, G.A., Aroush, D.R.B., Funari, S.S., Roschger, P., Wagner, H.D., Fratzl, P., 2005. Nanoscale deformation mechanisms in bone. Nano Lett. 5 (10), 2108–2111.
Guz, A.N., Checkhov, V.N., 1992. Stability of laminated composites. Appl. Mech. Rev. 45 (2), 81–101.
He, L.H., Swain, M.V., 2007. Influence of environment on the mechanical behaviour of mature human enamel. Biomaterials 28 (30), 4512–4520.
Hull, D., 1981. An Introduction to composite materials. Cambridge University Press, Cambridge.
Jackson, A.P., Vincent, J.F.V., Turner, R.M., 1988. The mechanical design of nacre. Proc. R. Soc. London Ser. B 234 (1277), 415–&..
Jager, I., Fratzl, P., 2000. Mineralized collagen fibrils: a mechanical model with a staggered arrangement of mineral particles. Biophys. J. 79 (4), 1737–1746.
Ji, B., Gao, H., 2004a. A study of fracture mechanisms in biological nano-composites via the virtual internal bond model. Mater. Sci. Eng. A—Struct. Mater. 366 (1), 96–103.
Ji, B., Gao, H., 2006. Elastic properties of nanocomposite structure of bone. Compos. Sci. Technol. 66 (9), 1212–1218.
Ji, B., Gao, H., 2010. Mechanical principles of biological nanocomposites. Annu. Rev. Mater. Res. 40, 77–100.
Ji, B., Gao, H., Hsia, K.J., 2004. How do slender mineral crystals resist buckling in biological materials? Philos. Mag. Lett. 84 (10), 631–641.
Ji, B.H., Gao, H.J., 2004b. Mechanical properties of nanostructure of biological materials. J. Mech. Phys. Solids 52 (9), 1963–1990.
Jones, R., 1975. Mechanics of composite materials. McGraw-Hill, New York.
Kamat, S., Su, X., Ballarini, R., Heuer, A.H., 2000. Structural basis for the fracture toughness of the shell of the conch *Strombus gigas*. Nature 405 (6790), 1036–1040.
Katti, D.R., Katti, K.S., Sopp, J.M., Sarikaya, M., 2001. 3D finite element modeling of mechanical response in nacre-based hybrid nanocomposites. Comput. Theor. Polym. Sci. 11 (5), 397–404.
Katti, K.S., Katti, D.R., 2006. Why is nacre so tough and strong? Mater. Sci. Eng. C—Biomim. Supramol. Syst. 26 (8), 1317–1324.
Kauffmann, F., Ji, B.H., Dehm, G., Gao, H.J., Arzt, E., 2005. A quantitative study of the hardness of a superhard nanocrystalline titanium nitride/silicon nitride coating. Scr. Mater. 52 (12), 1269–1274.
Landis, W.J., 1995. The strength of a calcified tissue depends in part on the molecular-structure and organization of its constituent mineral crystals in their organic matrix. Bone 16 (5), 533–544.
Landis, W.J., Hodgens, K.J., Song, M.J., Arena, J., Kiyonaga, S., Marko, M., Owen, C., McEwen, B.F., 1996. Mineralization of collagen may occur on fibril surfaces: evidence from conventional and high-voltage electron microscopy and three-dimensional imaging. J. Struct. Biol. 117 (1), 24–35.
Liu, G., Ji, B., Huang, K.-C., Khoo, B.C., 2011. Analytical solutions of the displacement and stress fields of the nanocomposite structure of biological materials. Compos. Sci. Technol. 71, 1190–1195.

Mayer, G., 2005. Rigid biological systems as models for synthetic composites. Science 310 (5751), 1144–1147.
Menig, R., Meyers, M.H., Meyers, M.A., Vecchio, K.S., 2000. Quasi-static and dynamic mechanical response of *Haliotis rufescens* (abalone) shells. Acta Mater. 48 (9), 2383–2398.
Menig, R., Meyers, M.H., Meyers, M.A., Vecchio, K.S., 2001. Quasi-static and dynamic mechanical response of *Strombus gigas* (conch) shells. Mater. Sci. Eng. A—Struct. Mater. Prop. Microstruct. Process. 297 (1–2), 203–211.
Parnes, R., Chiskis, A., 2002. Buckling of nano-fibre reinforced composites: a re-examination of elastic buckling. J. Mech. Phys. Solids 50 (4), 855–879.
Rho, J.Y., Kuhn-Spearing, L., Zioupos, P., 1998. Mechanical properties and the hierarchical structure of bone. Med. Eng. Phys. 20 (2), 92–102.
Rosen, B.W., 1964. Mechanics of composite strengthening. In: Spencer H. Bush (Ed.), Fiber Composite Materials. American Society of Metals, Cleveland, OH, pp. 37–75.
Schuerch, H., 1966. Prediction of compressive strength in uniaxial boron fiber–metal matrix composite material. AIAA J. 4 (1), 102–106.
Su, Y., Ji, B., Zhang, K., Gao, H., Huang, Y., Hwang, K., 2010. Nano to micro structural hierarchy is crucial for stable superhydrophobic and water-repellent surfaces. Langmuir 26 (7), 4984–4989.
Su, Y., Wu, J., Fan, Z., Hwang, K., Song, J., Huang, Y., Rogers, J., 2012. Postbuckling analysis and its application to stretchable electronics. J. Mech. Phys. Solids 60 (3), 487–508.
Tesch, W., Eidelman, N., Roschger, P., Goldenberg, F., Klaushofer, K., Fratzl, P., 2001. Graded microstructure and mechanical properties of human crown dentin. Calcif. Tissue Int. 69 (3), 147–157.
Wang, R.Z., Suo, Z., Evans, A.G., Yao, N., Aksay, I.A., 2001. Deformation mechanisms in nacre. J. Mater. Res. 16 (9), 2485–2493.
Warshawsky, H., 1989. Organization of crystals in enamel. Anat. Rec. 224 (2), 242–262.
Zhang, Z., Zhang, Y.W., Gao, H., 2011. On optimal hierarchy of load-bearing biological materials. Proc. R. Soc. B: Biol. Sci. 278 (1705), 519–525.
Zuo, S.C., Wei, Y.G., 2008. Microstructure observation and mechanical behavior modeling for limnetic nacre. Acta Mech. Sin. 24 (1), 83–89.